Real time dynamics of colliding gauge fields and the ''glue burst''

W. Pöschl and B. Müller
Department of Physics, Duke University, Durham, North Carolina 27708-0305
(Received 22 December 1998; published 3 November 1999)

The Yang-Mills equations provide a classical mean field description of gauge fields. In view of developing a coherent description of the formation of the quark gluon plasma in high energetic nucleus-nucleus collisions we study pure gauge field dynamics in $3+1$ dimensions. In collisions of wave packets, numerically simulated on a SU(2) gauge lattice, we study transverse and longitudinal energy currents. For wave packets with different polarizations in color space, we observe a time-delayed fragmentation after the collision resulting in a rapid expansion into transverse directions. We call this phenomenon the ''glue burst.'' An analysis of the Yang-Mills equations reveals the explanation for this behavior. It is pointed out that this effect could play a role in ultrarelativistic heavy-ion collisions. [S0556-2821(99)00521-4]

PACS number(s): 12.38.Gc, 02.60.Cb, 05.45.−a, 42.25.Fx

I. INTRODUCTION

It is one of the most challenging topics in the theory of ultrarelativistic heavy-ion collisions to develop a coherent description of the formation of the quark gluon plasma that is based on quantum chromodynamics (QCD). Various QCD-based models for the time evolution of such collisions have been developed in recent years [1–6]. These models are based on the idea of a perturbative scattering of particles within transport models and describe in principle the evolution of a collision from the first contact of the nuclei throughout the high density phase until the beginning of hadronization. These models however contain still a variety of problems. One of the problems concerns the description of the initial state of the colliding nuclei. The transport equations start from probability distributions of partons in the phase space. In reality, however, the states of the nuclei are described through coherent parton wave functions. The incoherent parton description especially breaks down at exchanges of small transverse momenta.

McLerran and Venugopalan proposed [7] that the proper solution of these difficulties is the perturbative expansion not around the empty QCD vacuum but around a vacuum of the mean color fields which accompany the quarks in the colliding nuclei. In recent years, they and their collaborators [8,9]) have developed an effective coherent description of the glue field dynamics at central rapidities. Their model allows for solving the Yang-Mills equations in $2+1$ dimensions within a static light cone source model and provides classical coherent solutions on a gauge lattice in the transverse plane at the center of collision [10]. The basic idea of this approach motivates the development of a combination of the parton cascade model [3] with a coherent description of the initial states.

Recently, we have proposed a combination of a gauge lattice description for the soft color fields with a transport model for color charged particles [11]. Leaving out the collision terms first, this model then has been applied to simulate the collision of clouds of color charged particles accompanied by soft color fields in $3+1$ dimensions [12]. The field energy distributions obtained for times shortly after the collision have shown transverse energy flows resulting from glue field scattering in the center of collision. For times larger than 1 fm/c glue field radiation seemed to be dominant. The sudden appearance of transverse energy flows during the overlap time of the nuclei was the motivation to study here the pure glue mean field dynamics leaving out the particles.

The time evolution of colliding Yang-Mills field wave packets was studied a few years ago in $1+1$ dimensions [13]. These calculations have shown that wave packets of parallel polarization in color space (Abelian case) do not interact whereas wave packets polarized in different color directions (non-Abelian case) decay after the collision into low frequency modes. This mechanism of a coupling between high-frequency short-wavelength modes and low-frequency long-wavelength modes in the Yang-Mills equations was first observed in numerical simulations of decay of slightly perturbed standing Yang-Mills waves [14].

In the present paper, we focus on the transverse dynamics and the coupling between longitudinal and transverse energy flows in collisions of localized Yang-Mills field configurations. A study of the transverse dynamics requires simulations in at least $2+1$ dimensions. Subsequently, we describe the method used to solve the Yang-Mills equations and present results obtained from collisions simulated in $3+1$ dimensions on a SU(2) gauge lattice. These studies also reveal an interesting behavior of the time-evolution of non-Abelian gauge fields.

II. TIME EVOLUTION ON THE GAUGE LATTICE

In the Lie algebra LSU(2), we define the adjoint gauge fields $\mathcal{A}^\mu(x) := A^\mu_c(x) T^c$ and the adjoint field strength tensor $\mathcal{F}^{\mu\nu} := F^{\mu\nu}_c T^c$. Einsteins sum convention has to be applied in the Euclidean metric for upper and lower color indices and in the Mincowski metric for upper and lower Greek indices. The symbols T^c with color index $c=1,2,3$ denote the generators of LSU(2) obeying the commutation relations $[T^a,T^b]_- = i f_{abc} T^c$ and hence $\mathcal{A}^\mu(x), \mathcal{F}^{\mu\nu}_{(x)} \in \mathrm{LSU}(2)$ for all $x \epsilon \mathbf{R}^4$. Here, we chose the representation $T^c = 1/2 \sigma^c$ with the Pauli matrices σ^c. Further below, we use also $T^0 := \frac{1}{2}\mathbf{1}_2$ which is linearly independent from the generators T^c. With

these conventions, we denote the Yang-Mills equations in the short form

$$[\mathcal{D}_\mu, \mathcal{F}^{\mu\nu}]_- = 0, \tag{1}$$

where $\mathcal{D}_\mu$ is defined

$$\mathcal{D}_\mu := \partial^\mu - igA^\mu. \tag{2}$$

With this definition of the covariant derivative $\mathcal{D}_\mu$ on the SU(2) main fold, and with the definitions $\mathcal{E}^\mu(x) := E_c^\mu(x)T^c$, $\mathcal{B}^\mu(x) := B_c^\mu(x)T^c$ $[\mathcal{E}^\mu(x), \mathcal{B}^\mu(x) \in \mathrm{LSU}(2)]$ of the adjoint color electric and color magnetic field quantities, the Yang-Mills equations Eq. (1) can be expressed in a form which resembles the U(1) Maxwell equations in the vacuum

$$[\vec{\mathcal{D}}, \vec{\mathcal{E}}]_- = 0, \tag{3}$$

$$[\vec{\mathcal{D}}, \vec{\mathcal{B}}]_- = 0, \tag{4}$$

$$[\vec{\mathcal{D}}\times, \vec{\mathcal{E}}]_- = [\mathcal{D}_0, \vec{\mathcal{B}}]_-, \tag{5}$$

$$[\vec{\mathcal{D}}\times, \vec{\mathcal{B}}]_- = [\mathcal{D}_0, \vec{\mathcal{E}}]. \tag{6}$$

With the condition $[\mathcal{A}(t,\vec{x}), \mathcal{A}(t,\vec{x}')]_- = 0$ for all $\vec{x}, \vec{x}' \in \mathbf{R}^3$ for one arbitrary real time t, the equations (3)–(6) become identical with the Maxwell equations. In this so-called Abelian [or U(1)] case, one expects a linear behavior of the solution and it therefore provides an important test through comparison with the solution in the general non-Abelian case. The Yang-Mills equations can be solved in an efficient manner on a gauge lattice in a Hamiltonian framework where we choose the temporal gauge $\mathcal{A}^0 = 0$.

A lattice version of the continuum Yang-Mills equations is constructed by expressing the color field amplitudes as elements of the corresponding Lie algebra, i.e., $\mathcal{E}_{\vec{x},k}, \mathcal{B}_{\vec{x},k} \in \mathrm{LSU}(2)$ at each lattice site $\vec{x}$. Subsequently, we use the index symbols $j,k,l = 1,2,3$ for the directions in the Euclidian subspace $\mathbf{R}^3$. On the lattice the following variables are defined:

$$\mathcal{U}_{\vec{x},l} = \exp[-iga_l \mathcal{A}_l(x)] = \mathcal{U}^\dagger_{\vec{x}+l,-l}, \tag{7}$$

$$\mathcal{U}_{\vec{x},kl} = \mathcal{U}_{\vec{x},k}\mathcal{U}_{\vec{x}+k,l}\mathcal{U}_{\vec{x}+k+l,-k}\mathcal{U}_{\vec{x}+l,-l} \tag{8}$$

In adjoint representation the color electric and color magnetic fields are expressed in terms of the above defined link variables $\mathcal{U}_{\vec{x},l}$ and plaquette variables $\mathcal{U}_{\vec{x},kl}$ in the following way:

$$\mathcal{E}_{\vec{x},j} = \frac{1}{iga_j}\dot{\mathcal{U}}_{\vec{x},j}\mathcal{U}^\dagger_{\vec{x},j}, \tag{9}$$

$$\mathcal{B}_{\vec{x},j} = \frac{i}{4ga_k a_l}\epsilon_{jkl}(\mathcal{U}_{\vec{x},kl} - \mathcal{U}^\dagger_{\vec{x},kl}). \tag{10}$$

The lattice constant in the spatial directions $l = 1,2,3$ is denoted by a_l. As one can see from Eq. (7), the gauge field $\mathcal{A}_{\vec{x},l}$ is expressed in terms of the link variables $\mathcal{U}_{\vec{x},l} \in \mathrm{SU}(2)$, which represent the parallel transport of a field amplitude from a site $x \in X$ to a neighboring site $(x+l) \in X$ in the direction l. We choose $\mathcal{U}_{\vec{x},l}$ and $\mathcal{E}_{\vec{x},l}$ as the basic dynamic field variables and numerically solve the following equations of motion:

$$\dot{\mathcal{U}}_{\vec{x},k}(t) = iga_k \mathcal{E}_{\vec{x},k}(t)\mathcal{U}_{\vec{x},k}(t), \tag{11}$$

$$\dot{\mathcal{E}}_{\vec{x},k}(t) = \frac{i}{2ga_1a_2a_3}\sum_{l=1}^{3}\{\mathcal{U}_{\vec{x},kl}(t) - \mathcal{U}^\dagger_{\vec{x},kl}(t) - \mathcal{U}^\dagger_{\vec{x}-l,l}(t)[\mathcal{U}_{\vec{x}-l,kl}(t) - \mathcal{U}^\dagger_{\vec{x}-l,kl}(t)]\mathcal{U}_{\vec{x}-l,l}(t)\}. \tag{12}$$

III. CALCULATIONAL PROGRAM

In order to guide the reader through the remaining sections of this manuscript, we here first explain the calculational program the results of which will be reported in the remainder of our paper. The program has two major parts. In the first part, our goal is to establish contact with the results reported by Hu *et al.* [13] on collisions of Gaussian wave packets of Yang-Mills fields in on spatial dimension. Those results showed that the interactions of two counterpropagating wave packets are strongly inelastic whenever the orientations of the color vectors are not exactly parallel.

Because we are here studying Yang-Mills dynamics on three-dimensional lattices, we will choose initial conditions that resemble those of Ref. [13] as closely as possible, yet involve two transverse dimensions. Our two counterpropagating wave packets are chosen to have a Gaussian shape in the longitudinal direction and no dependence at all in the other two spatial directions. In other words, we study collisions of plane wave packets with a Gaussian longitudinal profile. (These wave packets would be similar to ultrashort pulses of nearly monochromatic light emitted by a femtosecond laser.) We do not claim that this calculation (for Yang-Mills fields) bears close semblance to any situation that could occur in practice, but it is purely for comparative purposes.

The wave packets are characterized by the average longitudinal wave number $\overline{k_3}$, the Gaussian width Δk_3 of the wave packet in Fourier space, the intensity of the plane wave packet, and their polarization in real and in color space. We express the intensity of the wave packets in terms of a parameter σ, denoting the cross sectional area containing the amount of energy equal to a single field quantum. It will be of importance to understand whether the wave packet interactions correspond to a regime of weak coupling or not. The condition for weak coupling is $gA^2 \ll \overline{k_3}A$ or $aA/\overline{k_3} \ll 1$, where A is the amplitude of the wave packet. For the parameter choices of the following section ($\overline{k_3}a = \pi/2$, $\Delta k_3 a = \pi/100$, $\sigma = 100a^2$) this condition reads

$$\frac{gA}{\overline{k_3}} = \frac{g}{25\pi^{5/4}} \ll 1, \tag{13}$$

and thus is satisfied for all considered values of the coupling constant ($g \leqslant 14$). Therefore, we do not expect that our results presented below are contaminated by lattice artifacts.

As will be seen in the next section, our results do not deviate drastically from those of Hu *et al.* [13]. Colliding wave packets with essentially nonabelian polarization interact inelastically. Part of the energy initially residing in the longitudinal motion is transferred into transverse degrees of freedom (this effect could, of course, not be studied by the previous authors who considered only one-dimensional dynamics). The time between initial interaction and clear emergence of the inelasticity grows with decreasing value of g in a manner consistent with results from other studies of the dynamical instabilities of real-time Yang-Mills fields [14]. While the presence of transverse dimensions obviously changes the quantitative results in comparison with the previous one-dimensional analysis, the results are qualitatively similar. The interaction of the two colliding wave packets is analyzed in detail perturbatively in the two appendixes. There we show analytically how, in the limit of weak coupling, transverse degrees of freedom of the Yang-Mills field are excited by the interactions of two plane wave packets, and that the time required for the full development of the scattered components grows as g^{-2}.

In the second part of our numerical program, we study the collision of two wave packets that are spatially localized in one of the two transverse dimensions. We still consider Gaussian longitudinal profiles, not because we believe that they are physically realistic, but rather so that we do not change too many properties of the interacting waves at once. The transverse localization allows us, for the first time, to investigate the decoherence of individual components of the wave packets in the transverse direction, as it must occur in any truly three-dimensional scattering event. This was still impossible in the cases of the first part of our present study, because of the transverse homogeneity of the wave packets.

The results of our numerical calculations show that the transverse dimensions play a much more significant role for finite size wave packets. The main effect of the interaction among the two wave packets no longer appears to be simply the excitation of transverse field components, but the total disintegration of the wave packets themselves. We have not been able to analyze this effect in detail analytically, but our numerical results are consistent with the rapid break-up of the coherent wave packets into localized field lumps at a certain time after the initial interaction.

It may appear puzzling why the disintegration occurs with a significant time delay. For this we note that the wave packets propagate essentially with the speed of light (except for a slight delay due to lattice artefacts of the dispersion relation). The appearance of any disturbance in the structure of the wave packet is thus highly time dilated when viewed from the center-of-momentum frame. The decoherence of the different components of the perturbed wave packets occurs with a long delay, just as in the case of radiation by a fast-moving charged particle, where the delay is known as the Landau-Pomeranchuk-Migdal effect [15]. It would be interesting to analyze the phenomenon reported below in terms of these concepts, but we have not yet done so.

IV. NUMERICAL RESULTS

A. Collision of plane wave packets

First, we study the collision of plane wave packets which have initially constant amplitude in the transverse planes of a three-torus lattice implying periodic boundary conditions.[1] The size is chosen $20\times 20\times 2000$ lattice points. We denote the lattice spacing in the space direction l by a_l. For a collision, we initially arrange wave packets of a Gaussian shape in the longitudinal direction.[2] The average momenta of the wave packets are $(0,0,\pm\overline{k}_3)$ and their momentum spread is denoted Δk_3. As a consequence of the lattice discretization these quantities are restricted to values between the maximal and minimal Fourier-momenta on the lattice:

$$k_l^{\min}=\frac{\pi}{(N_l a_l)}, \quad k_l^{\max}=\frac{\pi}{(N_l a_l)}, \tag{14}$$

$$k_l^{\min} \ll \Delta k_l \ll \overline{k}_l \ll k_l^{\max}. \tag{15}$$

The polarization in color space is defined by the unit vectors $\vec{n}_L$ for the left (L) and $\vec{n}_R$ for the and right (R) moving wave packet, respectively. The polarization in coordinate space is expressed by Kronecker symbols $\delta_{l,k}$.

We express the initial conditions through the gauge fields

$$A^c_{l,L}=\delta_{l1} n^c_L \phi(+t, x_3 - Z_L), \tag{16}$$

$$A^c_{l,R}=\delta_{l1} n^c_R \phi(-t, x_3 - Z_R), \tag{17}$$

where the scalar function $\phi(t,x_3)$ defines the initial wave packet

$$\phi(t,x_3)=\phi_0 \exp\left(-\frac{1}{2}\Delta k_3^2 (t+x_3)^2\right)\cos[\overline{k}_3(t+x_3)], \tag{18}$$

$$\phi_0=\sqrt{(2\Delta k_3)/(\sqrt{\pi}\sigma\overline{k}_3)}\,(1+e^{-(\overline{k}_3/\Delta k_3)^2}). \tag{19}$$

The amplitude factor ϕ_0 is determined for a normalized wave packet when $\sigma = 100 a_1 a_2$. The parameter σ is used to control the amplitude and allows to adjust the energy contained in a wave packet. In a particle interpretation it describes the total cross section per particle contained in the wave packet [13]. The second term in ϕ_0 is usually negligibly small for wave packets since $\overline{k}_3/\Delta k_3 \gg 1$. We chose the

[1]The periodic boundary conditions are a consequence of the torus topology. In the computer program, the index i_l of the lattice sites runs from 0 to $N_l - 1$. When i_l reaches the value N_l, it is set to $i_l = 0$.

[2]Gaussian wave packets are taken for reasons of simplicity. We believe that the main features of the results presented in this paper do not depend on the detailed shape of the colliding wave packets. This expectation is supported by a recent calculation which shows a time-delayed sudden increase of the transverse energy currents for colliding field configurations of a very different shape [16].

polarizations in color space $\vec{n}_R=\vec{n}_L=(0,0,1)$ for the Abelian case and $\vec{n}_R=(0,0,1)$, $\vec{n}_L=(0,1,0)$ for the non-Abelian case. Once the initial fields are mapped on the lattice, the time evolution of the collision starts from the superposed initial conditions

$$\mathcal{U}^{(0)}_{x,l}=\mathcal{U}^{(0)}_{x,l,L}\cdot\mathcal{U}^{(0)}_{x,l,R}, \tag{20}$$

$$\mathcal{E}^{(0)}_{x,l}=\mathcal{E}^{(0)}_{x,l,R}+\mathcal{E}^{(0)}_{x,l,L}, \tag{21}$$

respectively. A linear superposition of solutions obeys the Yang-Mills equations only if these solutions have no overlap. Therefore, the initial separation ΔZ should be much larger than $1/\Delta k_3$.

The calculation contains four parameters. The relative color polarization which is parameterized by the angle θ_C defined through $\vec{n}_L\cdot\vec{n}_R=\cos(\theta_C)$. The average momentum of the wave packets $\overline{k}$ and their width Δk_3 and the coupling constant g which can be rewritten in terms of the parameter σ as $g'=g/\sqrt{\sigma}$ by simultaneously rescaling the field $\mathcal{A}$ as $\mathcal{A}'=\sqrt{\sigma}\mathcal{A}$. Consequently, the system shows the same dynamics for different values of g and σ, as long as the ratio $g'=g/\sqrt{\sigma}$ is kept fixed. Multiplying the Eq. (33) in Sec. IV by a factor g, shows that each amplitude $\mathcal{A}^\mu$ absorbs a g such that no g is left over in Eq. (33). For $\overline{k_3}\gg\Delta k_3$, the energy contained in one wave packet is essentially $\overline{k_3}/\sigma$, i.e., for given $\overline{k_3}$ the energy is determined through the amplitude and vice versa the amplitude is thus fixed by the energy. Once the amplitude is fixed, it makes sense to use the coupling constant as an additional parameter which determines the reaction dynamics of colliding wave packets. This is preferable also in view of studies in the future where normalized Dirac fields or color charged classical particles shall be included. In such cases g appears also in front of the source current of the inhomogeneous Yang-Mills equations. We therefore keep the explicit denotation of g in the subsequent sections.

In the following we present results from a simulated collision in the non-Abelian case with the parameters $\overline{k_3}=\pi/(2a_3)$, $\Delta k_3=\pi/(100a)$, $g=1$, $\sigma=100a^2=1.0$ fm^2. The simulation was performed on a uniform lattice with constants $a_1=a_2=a_3=a$ using a time step size $\Delta t=a/10$. If we would consider a collision of nuclei at low energies, $a=0.1$ fm would be an appropriate choice for the above parameter settings. In particular, $\Delta k_3=\pi/(100a)$ corresponds thus to a FWHM (full width half maximum) of 10 fm which is approximately the diameter of a ^{208}Pb nucleus. It is important to note that for the above chosen values, the calculation runs in the regime of weak coupling.[3] Subsequently, we refer

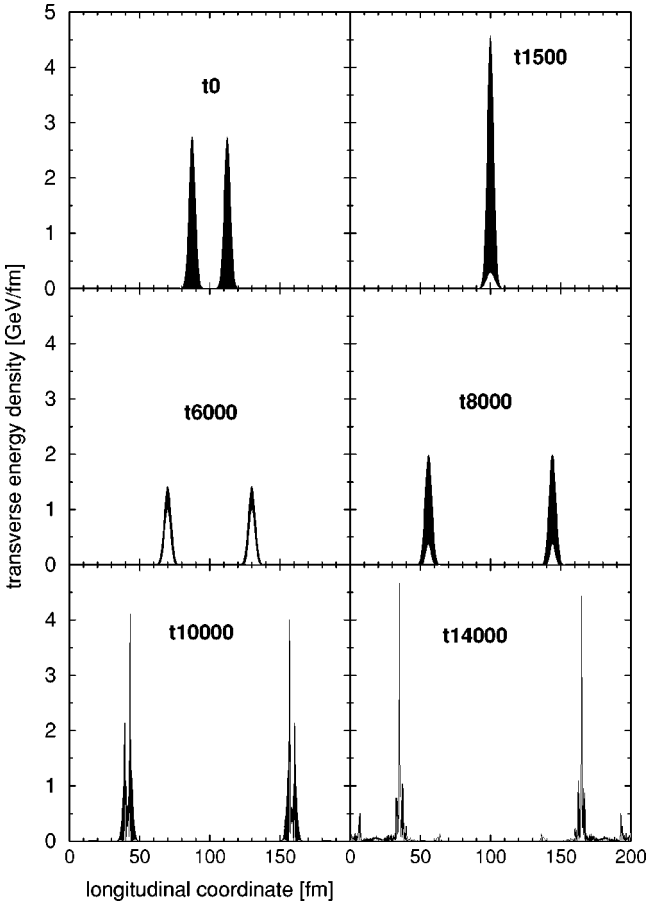

FIG. 1. Transverse energy densities $w^{(E)}_T(t,x_3)$ are plotted over the collision axis (longitudinal coordinate) for selected time steps t_n.

to the direction of the collision axis as the ''longitudinal direction'' and to directions perpendicular to the collision axis as the ''transverse directions.'' Accordingly, we define the transverse and longitudinal energy densities of the color electric field

$$w^{(E)}_T(t,x_3)=\int dx_1dx_2\sum_{l=1}^{2}\mathrm{Tr}[\mathcal{E}_l(t,\vec{x})\mathcal{E}_l(t,\vec{x})], \tag{22}$$

$$w^{(E)}_L(t,x_3)=\int dx_1dx_2\,\mathrm{Tr}[\mathcal{E}_3(t,\vec{x})\mathcal{E}_3(t,\vec{x})]. \tag{23}$$

Figure 1 displays $w^{(E)}_T$ plotted over the x_3 coordinate at various time steps t_n as indicated on top of the curves.

At initial time t_0 the distributions $w^{(E)}_T(t_0,x_3)$ of the wave packets are completely filled resulting from the strong oscillations in the longitudinal direction according to $\overline{k_3}=\pi/(2a_3)$. After 1500 time steps the wave packets are colliding and have reached maximum overlap. The smooth white zone at the bottom results from a phase shift between the two superposed waves, i.e., the maxima of the wave packet (1) to not coincide with the maxima of the wave packet (2) at time step t_{1500}. After the wave packets have

[3]By ''weak coupling'' on the lattice, it is understood that the phase angles $ga_lE^c_{x,l}\Delta t$ for each spatial direction l are much smaller than 2π. The link matrices are updated according to $\mathcal{U}_{x,l}(t+\Delta t/2)=\exp[-iga_l\mathcal{E}_{x,l}(t)\Delta t]\cdot\mathcal{U}_{x,l}(t-\Delta t/2)$. They have to obey the condition $\mathcal{U}_{x,l}(t+\Delta t/2)\simeq\mathbf{1}$. Further, the phase angles $0.5g\varepsilon_{jkl}a_ja_kB_{x,l}$ have to be small.

passed through each other (at about t_{2500}), a small white zone remains in the distribution $w_T^{(E)}(x_3)$ of each and keeps continuously growing. At time step t_{6000} ($t=600a$) the large fraction of the initial high frequency oscillations is reduced to a small remaining contribution visible on the surface of the distributions in Fig. 1. The height of the two receding humps decreases accordingly while the energy carried by each wave packet is constant in time. Almost all the energy which has originally been carried by short wavelength modes around $\overline{k_3}$ has been transmitted into long wavelength modes which have filled up the vallies in the oscillating distribution $w_T^{(E)}(x_3)$. This behavior agrees qualitatively with results obtained in Ref. [13] where collisions of wave packets have been studied on a one dimensional gauge lattice and for times not larger $t=600a$. At time step t_{8000}, however, we observe that energy is partly transmitted back into high frequent modes before the wave packets start to decay around time step t_{10000}. At time step t_{14000}, the energy distribution has expanded into longitudinal direction. The appearance of a circular polarization of the receding wave packets could in principle lead to the same behavior before they decay. This possibility, however, is excluded by our numerical results which show—in the case of plane waves—no excitation of modes with x_2 polarization for all times. This can be verified down to floating point precision but it has also a fully analytic explanation through Eq. (33) in Sec. IV for $\nu=2$.

This behavior does not appear in a collision of wave packets which are equally polarized in color space. In this case the shape of the two humps in the distribution $w_T^{(E)}(x_3)$ at the time step t_{14000} is almost identical to the shape at time t_0. Deviations result from lattice dispersion.

In Fig. 2, the corresponding longitudinal energy densities $w_L^{(E)}(t,x_3)$ are displayed on a logarithmic scale for selected time steps t_n. We remember that the wave packets were initially polarized into the transverse x_1 direction and consequently $w_L^{(E)}$ has to be zero as long as they propagate free. However, when the colliding wave packets of different color start overlapping, we observe an increasing longitudinal energy density in the overlap region around the center of collision at $x_3=100$ fm. Figure 2 clearly shows that $w_L^{(E)}(t,z)$ grows rather fast from time step t_{1000} until time step t_{1500} where it reaches a maximum and has grown by more than two orders of magnitude. For larger times the hump decreases again and practically disappears at t_{3000}. Around t_{6000}, however, the longitudinal energy density grows again at the positions of the receding wave packets. After 10000 time steps $w_L^{(E)}(z)$ has increased by five orders of magnitude.

A comparison of Fig. 1 with Fig. 2 indicates that the total color electric field energy on transverse links of the lattice decreases at large times while the total color electric field energy on longitudinal links increases. In order to understand this behavior in detail, we explore the time dependence of these quantities for different values of the coupling constant. To be more precise, we define the transverse and longitudinal energy of the color electric fields as

$$W_T^{(E)}(t)=\int dx_1 dx_2 dx_3 \sum_{l=1}^{2} \mathrm{Tr}[\mathcal{E}_l(t,\vec{x})\mathcal{E}_l(t,\vec{x})], \quad (24)$$

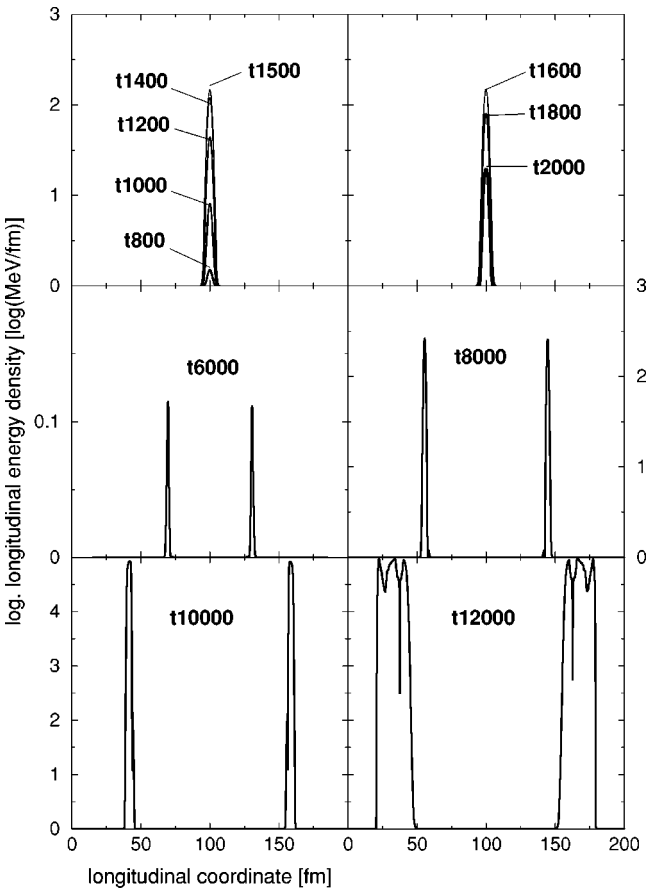

FIG. 2. Longitudinal energy densities $w_L^{(E)}(t,x_3)$ are plotted over the collision axis (longitudinal coordinate) for selected time steps t_n.

$$W_L^{(E)}(t)=\int dx_1 dx_2 dx_3 \,\mathrm{Tr}[\mathcal{E}_3(t,\vec{x})\mathcal{E}_3(t,\vec{x})]. \quad (25)$$

The integration in the definitions (24) and (25) is carried out over the whole lattice.

Figure 3 displays $W_T^{(E)}(t)$ over a time interval of $600a$ which corresponds to 6000 time steps. The energies are compared for different values of the coupling constant g. As already mentioned above, values of the coupling constant which differ from $g=1$ can be scaled out with the amplitude of the wave functions. The amplitude of wave packets, however, determines the energy carried by a wave. Once the energy is fixed by describing a real physical system, it makes sense to use different values of the coupling constant. Here, the collision is performed for wave packets which are normalized to $N_1N_2a^2/\sigma$ particles and we refer to different values of g.

Figure 3 shows that for small coupling, $W_T^{(E)}(t)$ remains unchanged through a long period of time after the collision which occurs in an interval around the time step t_{1500}. For $g=4$ the transverse color electric energy starts to decrease around time step t_{5000}. A comparison with curves obtained for increasing values of g shows that the $W_T^{(E)}(t)$ begins to decrease at earlier times. For the largest values $g=10,12,14$, the decrease begins in the overlap region of the

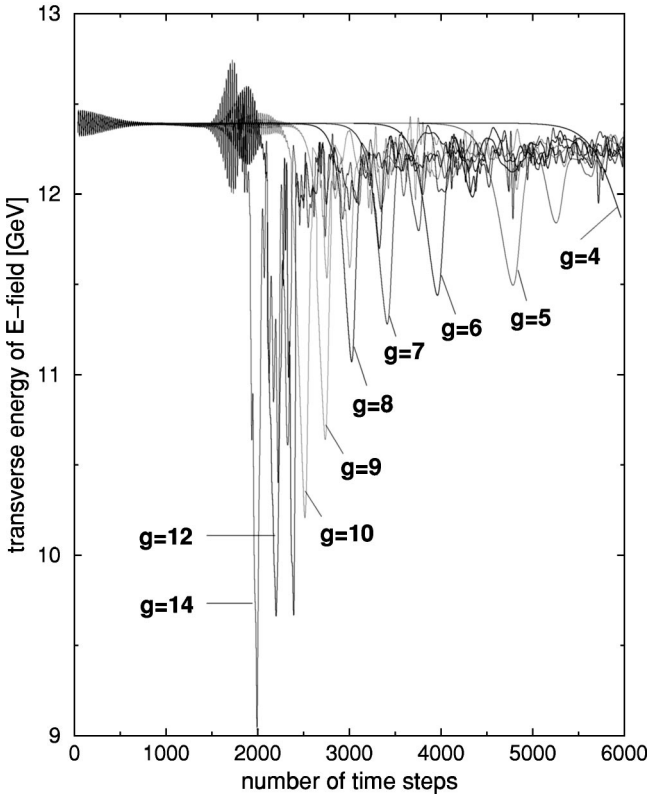

FIG. 3. The transverse color electric field energy $W_T^{(E)}(t)$ as a function of time is displayed for different values of the coupling constant g. The time step width of each time step is $\Delta t = a_3/10 = 0.01$ fm.

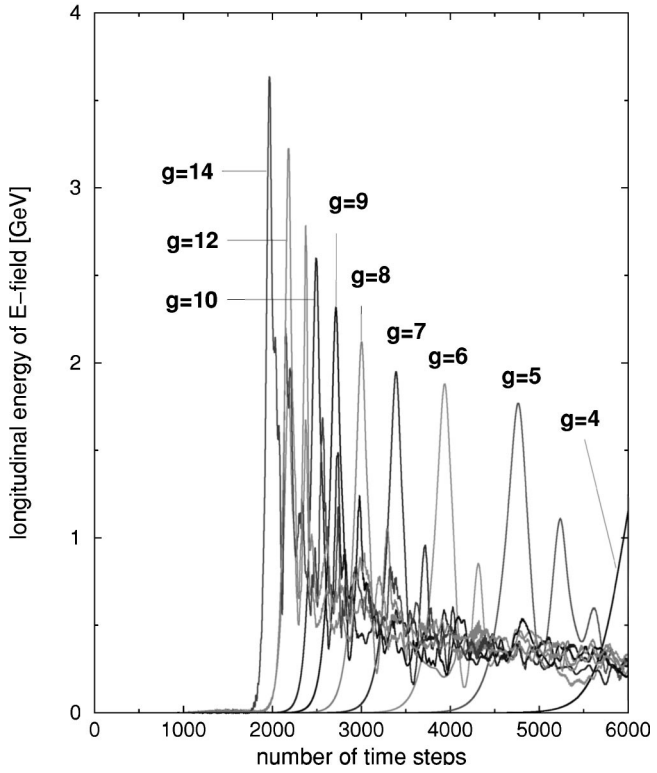

FIG. 4. The longitudinal color electric field energy $W_L^{(E)}(t)$ as a function of time is displayed for different values of the coupling constant g. The time step width of each time step is $\Delta t = a_3/10 = 0.01$ fm.

wave packets. In these cases, strong oscillations occur in the overlap region. The magnetic field energies $W_T^{(B)}(t)$ show a very similar behavior. The total energy of both wave packets is 24.76 GeV for our numerical choice $a = 0.1$ fm.

Figure 4 displays the corresponding longitudinal field energy $W_L^{(E)}(t)$. Before the wave packets start to overlap we find $W_L^{(E)}(t) = 0$ to a very high precision (10^{-26}). In the overlap region, a humplike structure occurs which grows for increasing values of g. For small values of g, $W_L^{(E)}(t)$ vanishes after the wave packets have passed through each other. After a long time $W_L^{(E)}(t)$ grows very steeply. Figure 4 shows clearly that the time between overlap and sudden growth shrinks for increasing coupling g. We find, that this time difference scales as $1/g^2$. Now the question arises whether the energy deposit in longitudinal links can be associated with fields propagating into transverse directions. To define energy currents, the Poynting vector is denoted in the adjoint representation

$$\vec{\mathcal{S}} := c\vec{\mathcal{E}} \times \vec{\mathcal{B}}. \tag{26}$$

With the transverse and longitudinal components of the vector (26) the total transverse and longitudinal energy currents are defined

$$i_T(t) := \sum_{l=1}^{2} \int dx_1 dx_2 dx_3 2 |\mathrm{Tr}[\mathcal{S}_l(t,\vec{x})]|, \tag{27}$$

$$i_L(t) := \sum_{l=3}^{3} \int dx_1 dx_2 dx_3 2 |\mathrm{Tr}[\mathcal{S}_l(t,\vec{x})]|. \tag{28}$$

These definitions may be applied in the regime of weak coupling to calculate the field energy currents.

In the following Fig. 5, we show the total transverse energy current $i_T(t)$ in the overlap time region for different values of the coupling constant. The figure shows that there is no transverse energy current before the wave packets start to overlap. In the overlap time region between the time steps t_{800} and t_{1500}, we observe a strong increase of the transverse energy current. The maximum is reached at time step t_{1500} where the overlap is maximal. At decreasing overlap in time region between t_{1500} and t_{2200}, $i_T(t)$ vanishes. The height of the humps increases for increasing values of g and scales as $1/g^2$. To become more precise, in the time region of the humps as shown in Fig. 5, the transverse current implies an oscillating structure of the time period $T_t = \bar{\lambda}/4$ over which we have averaged to obtain the smooth curves in Fig. 5. $\bar{\lambda}$ is here defined as $\bar{\lambda} = (2\pi)/k_3$. In the upper left panel in Fig. 5, we show an example for $\bar{k_3} = \pi/(4a_3)$ in the case $g = 8$ in which no averaging has been done. The curve displays a period of $T_t = 2a_3$ according to $\bar{\lambda} = 8a_3$. No averaging was necessary for times after the overlap time region.

Fig. 6 displays the same transverse energy currents as Fig. 5 but for a larger time interval and on a larger scale. Note that the current is plotted in units of $[i_T(t)] = c$ GeV in Fig. 6

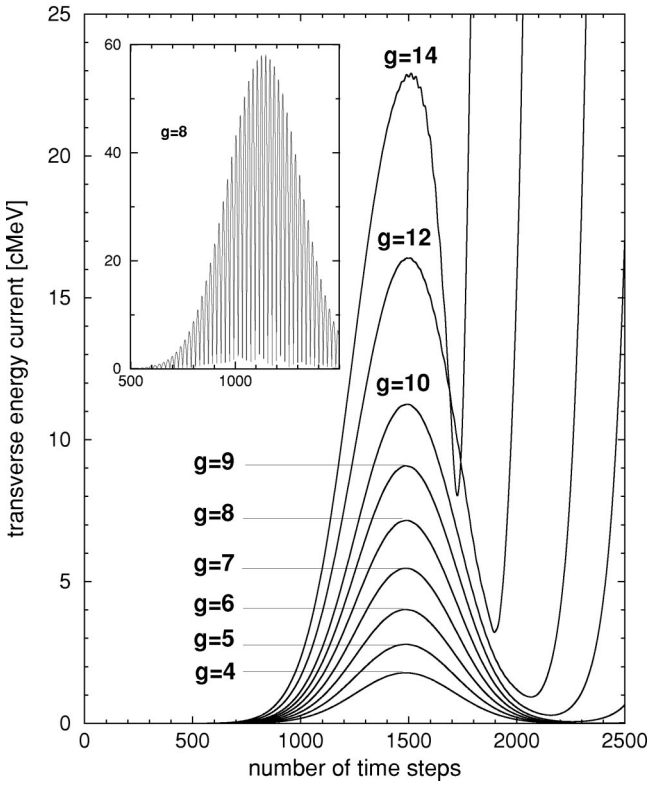

FIG. 5. The total transverse energy current $i_T(t)$ as a function of time is displayed for different values of the coupling constant g. The average longitudinal momentum of the colliding wave packets is $\overline{k_3}=\pi/(2a_3)$. In the upper left window, the full time-dependence of the transverse energy current is displayed at the example $g=8$ and $\overline{k_3}=\pi/(4a_3)$.

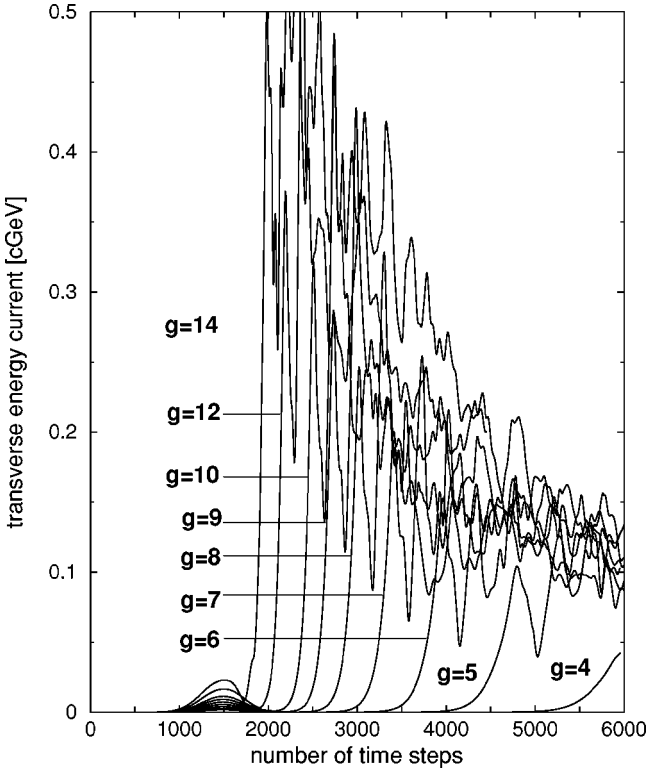

FIG. 6. Same as in Fig. 5 but for a larger time interval and on a larger scale for the transverse energy current $i_T(t)$.

but in units $[i_T(t)]=c$ MeV in Fig. 5. After passing through the hump region between time step t_{800} and t_{2000}, the energy current $t_T(t)$ disappears. For the smallest coupling $g=4$, it takes about 3500 time steps or $\tau\simeq 35$ fm from maximum overlap until to the point where i_T starts to regrow. This time, i_T grows to much larger values and stays large at later times. The time delay τ depends on $g,\Delta k_3,\overline{k_3}$. We find that $\tau\sim 1/g^2$ but haven't studied carefully the dependence on Δk_3 and $\overline{k_3}$. For large $\overline{k_3}$, one can argue analytically that $\tau\sim\overline{k_3}^{3/4}$. This will be further discussed in Appendix B. Some few calculations for smaller $\overline{k_3}$ have shown that τ increases monotonically for increasing $\overline{k_3}$. The sudden increase of i_T defines the ''glue burst.'' For large coupling it occurs already in the overlap region.

The following Fig. 7 displays the corresponding longitudinal energy currents $i_L(t)$. It shows that i_L decreases at the same time when i_T increases.

B. Collision of transverse finite wave packets

Subsequently, we present some results from the collision of wave packets with a finite transverse extent. We have carried out similar calculations as in the case of plane waves and found a similar, but even more pronounced behavior for the time dependence of the transverse and longitudinal en-

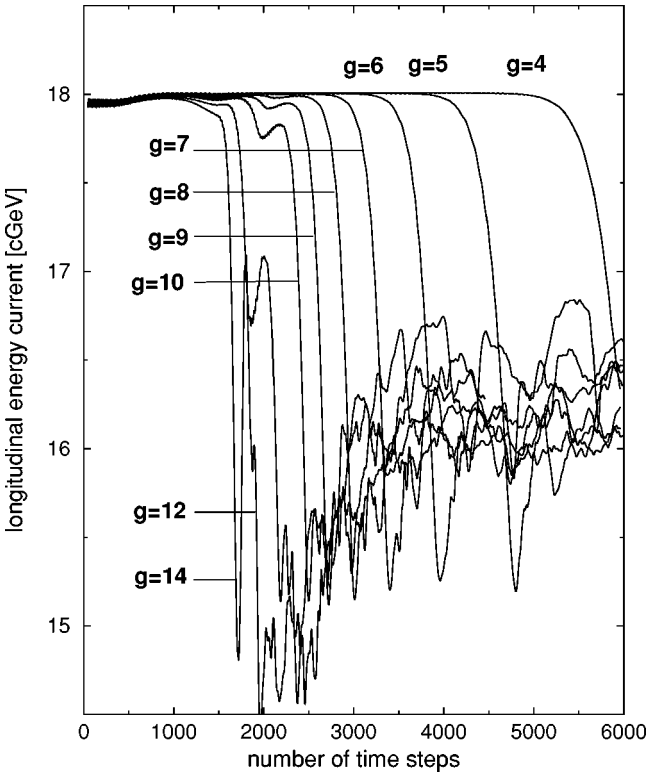

FIG. 7. The longitudinal energy currents $i_L(t)$ corresponding to the cases shown in Fig. 6 are displayed. $i_L(t)$ decreases at the same time when $i_T(t)$ increases.

ergy currents. Most of the calculations were carried out on a lattice of the size $4\times200\times800$ points. The wave packets have been initialized in the same way as in the case for plane wave packets. However, the initial wave functions depend now also on the transverse coordinates. Since a lattice with the same extension in both transverse directions would lead to an exceedingly large number of lattice points, we chose a small number of lattice points in the x_1 direction. Thus, we study the dynamics of a collision in the (x_2,x_3) plane integrated over the x_1 coordinate. Under these restrictions, the scalar function $\phi(t,x_2,x_3)$ defines the initial wave packet

$$\phi(t,x_2,x_3) := \phi_0 \exp\left(-\frac{1}{2}\Delta k_3^2 (t+x_3)^2\right) \times \exp[-(\Delta k_2 x_2)^\alpha]\cos[\bar{k_3}(t+x_3)], \quad (29)$$

$$\phi_0 := \sqrt{(2\Delta k_3)/(\sqrt{\pi}\sigma\bar{k_3})}. \quad (30)$$

The additional factor $\exp[-(\Delta k_2 x_2)^\alpha]$ describes the shape of the wave packet in the transverse x_2 direction. The parameter Δk_2 determines the transverse width and the parameter α controls the transverse shape. For large values of α, we obtain a sharp surface and the exponential tails are suppressed. Since the transverse extension of the lattice is limited, we choose the extension of the initial wave packet in the x_2 direction small enough to leave space for the transverse dynamics after the collision. Good values are $\Delta k_2 = 1/(40a_2)$ and $\alpha = 8$. The wave packet is thus 8 fm wide and extends over 80 lattice points into the main transverse direction. Further outside the amplitude is practically zero since α is large. For $\Delta k_3 = \pi/(100a_3)$, the full width at half maximum (FWHM) in longitudinal direction is 10 fm.

With the function $\phi(t,x_2,x_3)$ we determine the initial link variables and the color electric field amplitudes and map these data on the lattice at the initial positions of the wave packets. For a collision, the wave packets have opposite average momenta $\pm\bar{k_3}$. The evolution of the collision is carried out in the same way as for plane wave packets. Figure 8 shows snapshots of the transverse energy density of the color electric fields which we define as

$$w_T^{(E)}(t,x_2,x_3) = \int dx_1 \sum_{l=1}^{2} \mathrm{Tr}[\mathcal{E}_l(t,\vec{x})\mathcal{E}_l(t,\vec{x})]. \quad (31)$$

The simulation shown in Fig. 8 has been carried out for the non-Abelian case and with a coupling $g=6$. The other parameter settings are as for plane waves above. The upper left picture shows the distribution for the time step t_{100} where the shape has almost not changed as compared to the initial distribution. The wave packets decay into the transverse directions while they propagate free over the lattice. The upper right picture displays $w_T^{(E)}(t_{1500},x_2,x_3)$ at maximum overlap. In the middle left $w_T^{(E)}(t_{3500},x_2,x_3)$ is displayed. The distribution is almost identical with that obtained in the Abelian case at the same time step t_{3500}. At the time step t_{4000}, however, the waves packets start to burst in non-Abelian case. The last two images correspond to the time steps t_{5000} and t_{6000}.

In the Abelian case the wave packets continue to propagate undisturbed after the collision. Their time evolution agrees with that of a single wave packet sent from the left to the right or from the right to the left, respectively. The calculation has been repeated with different lattice sizes as for example on a $4\times300\times1000$ lattice and with smaller values for the time step width. No significant changes in the time evolution of the solution have been found. The possibility that boundary effects might lead to the time-delayed sudden decay is excluded. As already outlined above, the lattice is closed to the three-torus which implies periodic boundary conditions. Consequently, there are no points or links with exceptional conditions on the lattice. In the case of colliding plane waves, the symmetry under translation in transverse directions excludes boundary effects. The time-delayed sudden increase of the transverse field energy current appears in colliding plane waves which initially have different polarization in color space but it does not appear in the Abelian case which is identical with Maxwells field theory of U(1) gauge symmetry. The time-delayed burst in colliding wave packets of finite transverse extension, however, could result from small waves emitted into both transverse directions during the overlap time. Such waves could propagate around the lattice in transverse direction and collide again with the wave packets. There are two reasons excluding such a scenario. First, the time delay of the burst should then depend on the transverse number of lattice points. Such a dependence could not be found. Second, a transversely emitted perturbation does not reach again either wave packet since its speed is limited. On the other hand, the sudden increase of the transverse energy current after the collision exists in the non-Abelian case of colliding plane waves. It therefore exists also in collisions of transverse finite wave packets.

V. ANALYSIS OF THE YANG-MILLS EQUATIONS

In the following, we present the explanation of the glue burst solution by analyzing the Yang-Mills equations (1). The details of the discussion are presented in Appendix A. With the definition of the field tensor $\mathcal{F}^{\mu\nu} := \mathcal{D}^\mu \mathcal{A}^\nu - \mathcal{D}^\nu \mathcal{A}^\mu$, we rewrite Eq. (1) for the gauge fields in the adjoint denotation

$$[\mathcal{D}_\mu, (\mathcal{D}^\mu \mathcal{A}^\nu - \mathcal{D}^\nu \mathcal{A}^\mu)]_- = 0. \quad (32)$$

With the definition of the derivative $\mathcal{D}^\mu$ in Eq. (2) follows:

$$\partial_\mu \partial^\mu \mathcal{A}^\nu = \partial_\mu \partial^\nu \mathcal{A}^\mu + ig\partial_\mu[\mathcal{A}^\mu, \mathcal{A}^\nu]_- + ig[\mathcal{A}_\mu, \partial^\mu \mathcal{A}^\nu]_- - ig[\mathcal{A}_\mu, \partial^\nu \mathcal{A}^\mu]_- + g^2[\mathcal{A}_\mu, [\mathcal{A}^\mu, \mathcal{A}^\nu]_-]_-. \quad (33)$$

Since the time-delayed burstlike behavior of the solution occurs also in the case of colliding plane wave packets, we first consider this case. The phenomenon occurs in two steps. It is based on a delicate interplay of color degrees of freedom

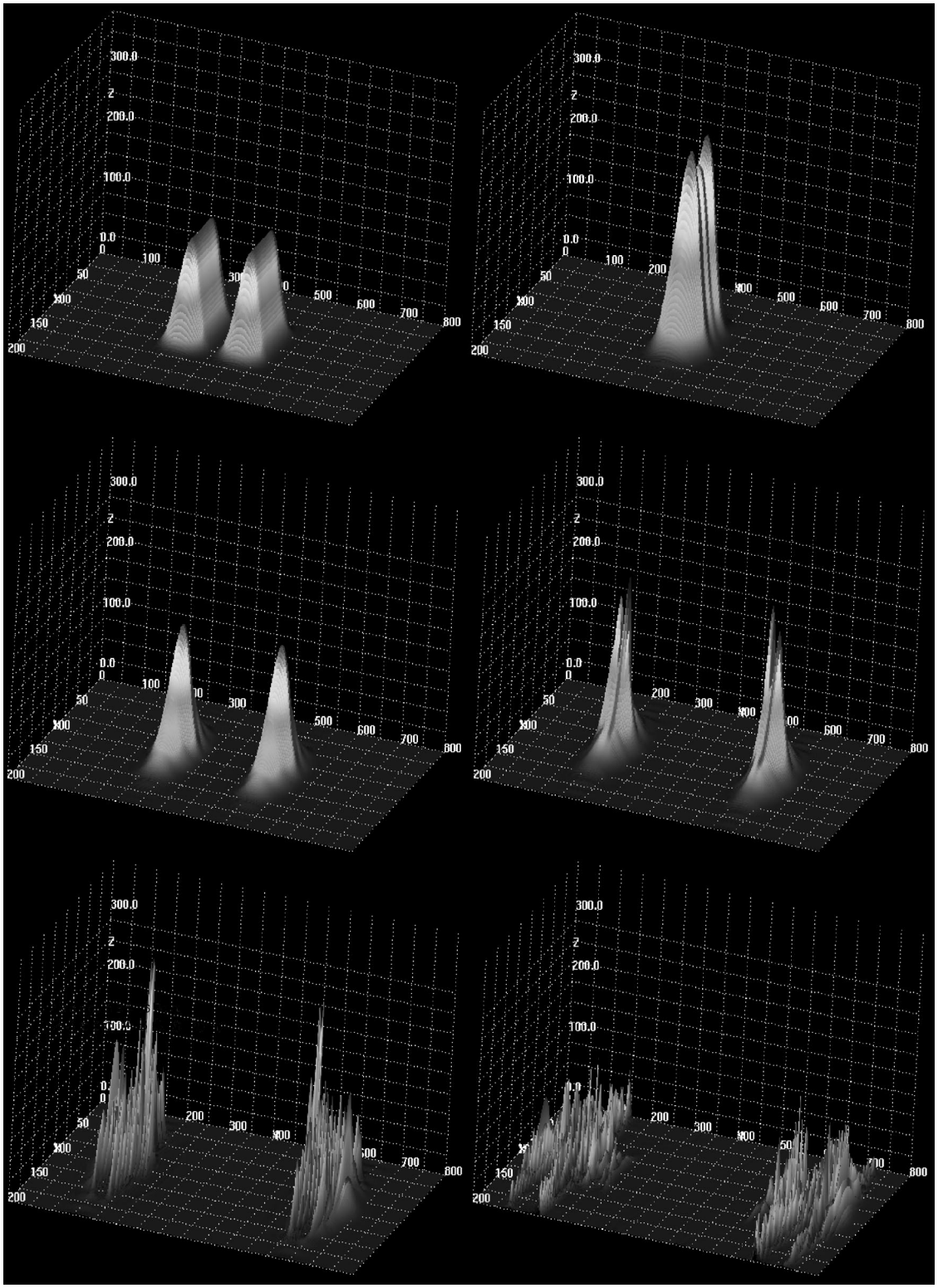

FIG. 8. The transverse color electric field energy density $w_T^{(E)}(t,x_2,x_3)$ is shown for six selected snapshots taken at the time steps t_{100}, t_{1500}, t_{3500}, t_{4000}, t_{5000}, and t_{6000}. The corresponding pictures are ordered from the upper left to the lower right.

between the color subspaces span(T_1,T_2) and span(T_3) and between transverse and longitudinal degrees of freedom in the field amplitudes.

The first step occurs in the overlap region of the wave packets in both, time and space. The Yang-Mills equations provide a mechanism which transfers field energy from transverse into longitudinal field degrees of freedom. It is explained by the equation for the longitudinal gauge field components which follows from Eq. (33) for $\nu=3$. For plane wave packets, only the fourth term and the g^2-term do not

vanish on the right-hand side (RHS) of Eq. (33) in the case $\nu=3$ and therefore the equation

$$\partial_\mu \partial^\mu \mathcal{A}^{(3)} = -ig[\mathcal{A}_\mu, \partial^{(3)} \mathcal{A}^\mu]_- + g^2 [\mathcal{A}_\mu, [\mathcal{A}^\mu, \mathcal{A}^{(3)}]_-]_- \tag{34}$$

describes the dynamics of the longitudinal fields $\mathcal{A}^{(3)}$ during the overlap time. In Eq. (34) and subsequently, we denote number values of the Lorentz indices in parentheses in order to distinguish them from number values of the color indices. The Greek symbols, however, are further on used without parentheses since it is clear from above that they denote Lorentz indices. A summation occurs only over upper and lower index symbols, not for numbers. For reasons of simplicity, we begin the discussion for the case where the longitudinal fields $\mathcal{A}^{(3)}$ remain small throughout the overlap time in comparison to the transverse fields of the initial wave packets. This implies that each color component in $\mathcal{A}^{(3)}$ is small. For initially polarized wave packets, as defined in the initial conditions in Sec. III, the above is equivalent to the assumption that the spatial components A_3^μ are small in the third color. The explanation is given in Appendix A.

For large enough $\overline{k_3}$, the time intervals in which the overlap within the period of one pair of overlapping oscillations increases are short, preventing $\mathcal{A}_{(3)}$ from becoming large. One can also argue, that for large k_3 both wave packets are located in widely separated regions in momentum space. The discussion of the mechanism provided by Eq. (39) shows that this large separation also prevents $\mathcal{A}_{(3)}$ from growing rapidly. Further, Δk_3 should not be too large since the overlap time of the wave packets (and thus $\mathcal{A}_{(3)}$) grows with Δk_3. Under these conditions, the field amplitudes obey the inequalities $|A_\mu^3 A_3^\mu| \ll |A_\mu^1 A_1^\mu|$ and $|A_\mu^3 A_3^\mu| \ll |A_\mu^2 A_2^\mu|$ during the overlap time. Consequently, terms on the RHS of Eq. (34) which contain amplitudes A_μ^3 are negligibly small. These terms contain factors T_1 and T_2, i.e., they contribute to the first and second color. For simplicity and briefness these small terms are neglected preliminary. The remaining terms on the r.h.s. act as source terms only for the third color component in $\mathcal{A}^{(3)}$ on the left-hand side (LHS) of (34) while the other color components remain zero. The remaining large terms on the RHS are

$$-ig[\mathcal{A}_\mu, \partial^3 \mathcal{A}^\mu]_- \simeq g(A_\mu^1 \partial^3 A_2^\mu - A_\mu^2 \partial^3 A_1^\mu) T_3, \tag{35}$$

$$\begin{aligned} g^2 [\mathcal{A}_{(1)}, [\mathcal{A}^{(1)}, \mathcal{A}^{(3)}]_-]_- = {} & g^2 A_{(1)}^1 A_1^{(1)} A_3^{(3)} T^3 \\ & - g^2 A_{(1)}^3 A_1^{(1)} A_3^{(3)} T^1 \\ & + g^2 A_{(1)}^2 A_2^{(1)} A_3^{(3)} T^3 \\ & - g^2 A_{(1)}^3 A_2^{(1)} A_3^{(3)} T^2. \end{aligned} \tag{36}$$

The validity of the above inequality has (for example) been well verified for the parameter values used in the calculation of the numerical results presented in the previous section. The results demonstrate that in the overlap time the longitudinal energy densities are smaller by at least one order of magnitude in comparison to the transverse energy densities.

In the region of $\overline{k_3}$, Δk_3 and g where the above inequalities do not hold, all terms on the RHS of Eq. (34) have to be taken into account in the discussion. The inclusion of the additional terms makes the discussion more involved since the color components $A_1^{(3)}$ and $A_2^{(3)}$ can no longer be neglected. This case will be considered further below. In cases for which the above inequalities are valid, the dynamics of the longitudinal fields in the overlap time is described in leading approximation, by the following equation:

$$\begin{aligned} \partial_0 \partial^0 \mathcal{A}^3 \simeq {} & g(A_\mu^1 \partial^3 A_2^\mu - A_\mu^2 \partial^3 A_1^\mu) T_3 + g^2 A_{(1)}^1 A_1^{(1)} A_3^{(3)} T^3 \\ & - g^2 A_{(1)}^3 A_1^{(1)} A_3^{(3)} T^1 + g^2 A_{(1)}^2 A_2^{(1)} A_3^{(3)} T^3 \\ & - g^2 A_{(1)}^3 A_2^{(1)} A_3^{(3)} T^2. \end{aligned} \tag{37}$$

The order g term on the RHS of Eq. (37) acts as a source term for the third color component of the longitudinal gauge field $\mathcal{A}^{(3)}(t,\vec{x})$. When the wave packets start to overlap, the space integral over this source term

$$I_3(t) := g \int d^3x [A_\mu^1(t,\vec{x}) \partial^{(3)} A_2^\mu(t,\vec{x}) - A_\mu^2(t,\vec{x}) \partial^{(3)} A_1^\mu(t,\vec{x})] \tag{38}$$

starts to grow. As Fig. 9 shows in a simplified manner, the derivative $\partial^{(3)} A_1^\mu$ is negative in the overlap region at the beginning and $\partial^{(3)} A_2^\mu$ is positive. Consequently, $I_3(t) > 0$ at times before the wave packets have reached maximum overlap. After the maximal overlap the derivatives change the sign and $I_3(t) < 0$.

Figure 9 displays in a qualitative manner the overlapping of two wave packets. The situation occurs in principle for each pair of overlapping oscillations (each taken between two minima) in colliding oscillating wave packets for which $\overline{k_3} > 0$. The corresponding time dependent behavior of the source current $I_3(t)$ at $\overline{k_3} = 0$ is depicted in Fig. 10. When the penetrating wave humps increase their overlap, the longitudinal contribution $I_3(t)$ to the source increases first. Since the derivative on the opposite side of both humps has opposite sign, the source term changes the sign as soon as the two humps have passed the maximum overlap. The discussion of step one in the collision applies in principle for each overlapping pair of wave humps where each hump of wave packet (1) passes through each hump of wave packet (2) during the collision.

As the source term $g(A_\mu^1 \partial^{(3)} A_2^\mu - A_\mu^2 \partial^{(3)} A_1^\mu)$ grows in time, the longitudinal gauge field $\mathcal{A}^{(3)}(t,\vec{x})$ grows. At the time of maximal overlap, the source current changes the sign and cancels the field $\mathcal{A}^{(3)}(t,\vec{x})$ as shown qualitatively by the dashed curve in Fig. 10.

During the whole time interval in which the wave packets pass through each other the finite longitudinal gauge field $\mathcal{A}^{(3)}(t,\vec{x})$ enters into the last term on the RHS of Eq. (33) leading to an additional but small contribution to the source term as long as g is not too large. For large g^2, the g^2 term

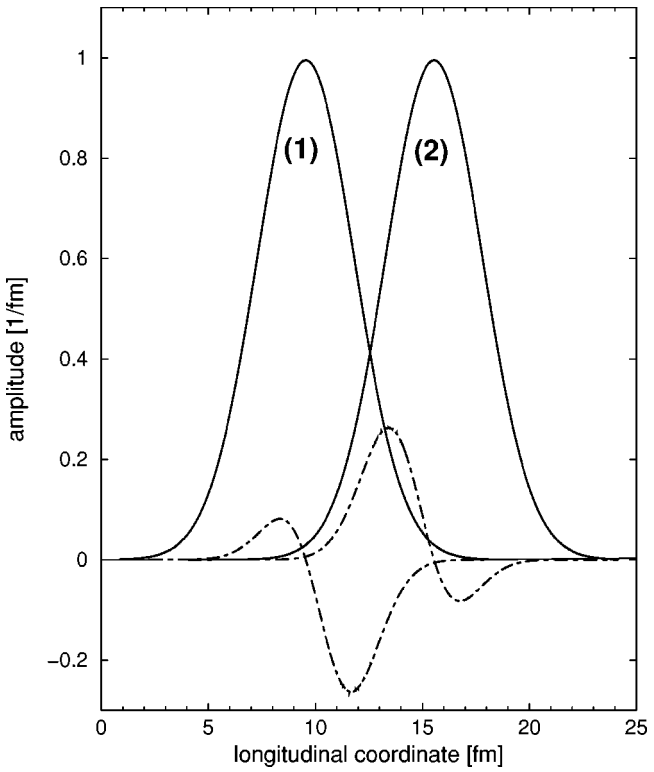

FIG. 9. Two colliding wave humps represented by gauge fields A_1 and A_2 at the beginning of the overlap. The wave packets are defined by $\phi(t,x_3)=\phi_0 \exp[-1/2\Delta k_3^2(t+x_3)^2]\cos[\overline{k_3}(t+x_3)]$ where only one hump is plotted for each in the range $(2n-1/2)\pi \leqslant k_3(t+x_3) \leqslant (2n+3/2)\pi$ between the positions of two minima. The minima are shifted to zero. The initial polarization is defined by the Eqs. (16) and (17). The products $A^1_\mu \partial^{(3)} A^\mu_2$ and $A^2_\mu \partial^{(3)} A^\mu_1$ (plotted as dashed lines) of the field amplitudes (solid lines) contribute to a source current in the longitudinal Yang-Mills equation.

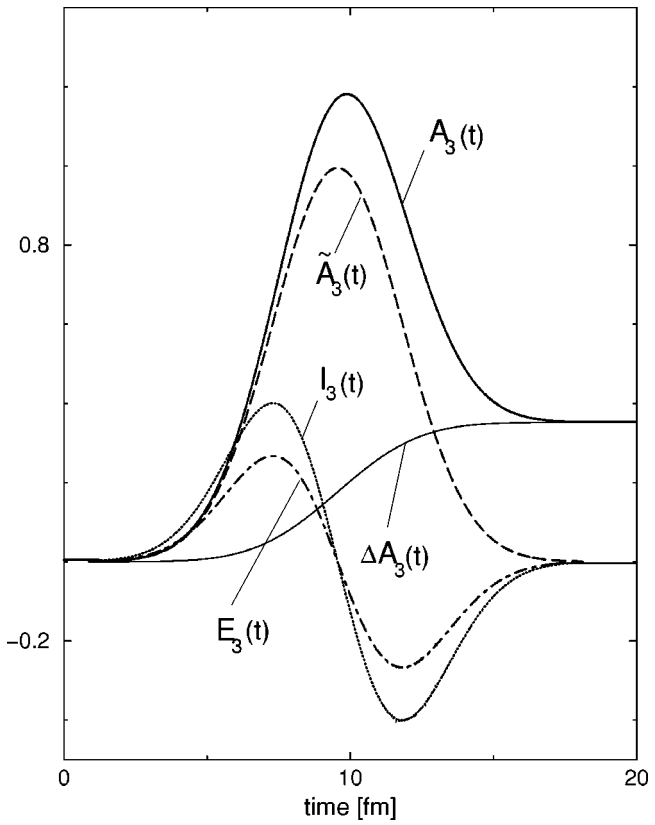

FIG. 10. The longitudinal contribution $I_3(t)$ to the source is plotted as a function of time (dotted line). The time dependence of the source term leads to a time dependence of the gauge field $\mathcal{A}_3$ as indicated by the dashed curve. The corresponding color electric field is indicated by the dot-dashed curve. The contribution from the g^2 term $\Delta\mathcal{A}_3(t)$ (solid line) adds to the gauge field resulting in the total field $\mathcal{A}_3(t)$ (fat solid line).

takes over during the overlap time as soon as the order g term has generated a finite amplitude $\tilde{\mathcal{A}}^{(3)}$. In this case, the burst occurs during the overlap phase. For large $\overline{k_3}$ and small Δk_3 the operator $\partial^{(3)}$ in the first RHS term of Eq. (37) is approximately replaced by a factor $\overline{k_3}$. This shows that the g term is larger than the g^2 term for not too large g. Indeed, our calculations show that for not too large values of g ($g<10$) and for small overlap times, i.e., small Δk_3, the contribution from the g^2-term remains small compared to the contribution resulting from the first source term on the rhs of Eq. (37). The g^2 term itself acts only as a weak source as long as $\mathcal{A}^{(3)}$ is small and it zero as long as $\mathcal{A}^{(3)}$ is zero. In particular $\mathcal{A}^{(3)}=0$ just before the beginning of the overlap. A finite longitudinal amplitude $A_3^{(3)}$ has first to be generated which is done by the fourth term on the rhs of Eq. (33) or the first term on the RHS of Eq. (37), respectively. This order g term acts as a initiator for the g^2 term. It also switches off again its contribution to the longitudinal gauge field when the wave packets have passed the maximum overlap. The fourth term goes to zero at vanishing overlap and does not contribute any further in the receding wave packets. However, the g^2 term causes a finite but small contribution $\Delta\mathcal{A}^{(3)}(t)$ to the longitudinal gauge field during the overlap time. The qualitative time dependent behavior of this contribution is shown by the solid line in Fig. 10. $\Delta\mathcal{A}^{(3)}(t)$ which is not canceled after the overlap is proportional to the surface under the dashed curve $[\tilde{\mathcal{A}}_{(3)}(t)]$ in Fig. 10. The fat solid curve depicts the time dependent behavior of the total longitudinal field $\mathcal{A}^{(3)}(t)$ while the dashed curve is obtained without g^2 term.

As a consequence of this mechanism, a small longitudinal field $\mathcal{A}^{(3)}(t,\vec{x})$ is left over in the receding wave packets. This contribution initiates the second step which forms the burst itself. Without restriction of the general case, we assume that the first wave packet is initially polarized in span(T_1) and the second wave packet is polarized in span(T_2). As soon as the wave packets obtain a small contribution in the gauge field component $A_3^{(3)}$, the spatial component $\mathcal{A}^{(1)}$ starts to change the polarization in color space. In wave packet (1) the components $A_2^{(1)}$ and $A_3^{(1)}$ grow whereas $A_1^{(1)}$ decreases accordingly. In wave packet (2) the components $A_1^{(1)}$ and $A_3^{(1)}$ grow whereas $A_2^{(1)}$ decreases accordingly. This behavior results in a rapid change of the T^3 terms on the rhs of Eq. (37). It is explained by the Yang-Mills equation for the first component which follows from Eq. (33) for $\nu=1$. Analyzing the RHS terms, we find

$$\partial_\mu \partial^\mu \mathcal{A}^{(1)} = -gA_1^{(1)}\partial_{(3)}A_3^{(3)}T^2 + gA_1^{(1)}\partial_{(3)}A_3^{(3)}T^1 - gA_3^{(3)}\partial_{(3)}A_1^{(1)}T^2 + gA_3^{(3)}\partial_{(3)}A_2^{(1)}T^1 + \cdots + g^2A_3^{(3)}A_3^{(3)}A_1^{(1)}T^1 + g^2A_3^{(3)}A_3^{(3)}A_2^{(1)}T^2 + \cdots, \tag{39}$$

where we denote only the most important contributions on the r.h.s. The first four terms on the RHS come from the second term on the RHS of Eq. (33). Similar contributions which come from the third term are omitted for brevity since they do not bring a new aspect into the discussion. The fourth term does not contribute for plane waves. The last two terms on the RHS of Eq. (39) come from the g^2 term. For details, we refer to Appendix A.

In the following we discuss the mechanism described by Eq. (39). The first, third, and sixth term on the RHS lead to excitations of modes in the color direction T^2 in the wave packet (1). The second, fourth and fifth term act in a similar manner for the wave packet (2). As long as $A_3^{(3)}$ is small, the contribution of the g^2 term is suppressed quadratically by $A_3^{(3)}$. This suppression is eventually enhanced by an additional factor $A_2^{(1)}$ with small Fourier components located around $+\overline{k_3}$. If these amplitudes exceed a certain strength, the g^2 term takes over to determine the dynamics of $A_2^{(1)}$ resulting in a fast growth of Fourier components at $+\overline{k_3}$. In the case of wave packet (1), these growing amplitudes $A_2^{(1)}$ and $A_3^{(3)}$ enter essentially into the third g^2 term on the RHS of Eq. (37) inducing the growth of $A_3^{(3)}$. In order to understand the time delay of the burst, the leading orders in the time dependence of the gauge fields are discussed for wave packet (1) shortly after the collision

$$A_2^{(1)} \simeq a_2^{(1)}t + b_2^{(1)}t^2 + \cdots, \tag{40}$$

$$A_3^{(3)} \simeq a_3^{(3)}t + b_3^{(3)}t^2 + \cdots. \tag{41}$$

Both amplitudes are zero in wave packet (1) before the overlap of the wave packets. $t=0$ defines here the begin of the overlap. In an exact treatment of colliding Gaussian wave packets, the begin of the overlap would be at $t=-\infty$. At large distances, however, the contributions from the nonlinear terms are strongly suppressed because in all contributing nonlinear terms, products appear between exponentially small amplitudes from one wave packet and finite amplitudes from the other wave packet. The alternating source term generates and recancels contributions to $\mathcal{A}^3$ almost perfectly within a period of oscillation because the perturbations caused by the g^2-term are threefold exponentially suppressed. $t=0$ can therefore be defined close to the full overlap of both wave packets. $t=0$ at a distance of two FWHM between centers the wave packets is sufficient because at that distance $A_3^{(3)}$ and $A_2^{(1)}$ are so small that the coefficients of order zero in the expansions of Eq. (40) and Eq. (41) can be neglected. These zero order coefficients decay exponentially for increasing initial distance and are therefore omitted in Eq. (40) and Eq. (41). Also numerical simulations on the lattice starting the collision from much larger distances do verify the above argumentation, i.e., $A_3^{(3)}$ is practically zero when the wave packets have approached to a distance of two FWHM.

We insert the expansions of Eq. (40) and Eq. (41) into the Yang-Mills equations and consider in leading powers the effects of the g^2 term on the $A_3^{(3)}$:

$$\partial_t \partial^t A_3^{(3)} \simeq -g^2 A_2^{(1)} A_3^{(3)} A_2^{(1)} + \cdots = -g^2 a_2^{(1)} a_3^{(3)} a_2^{(1)} t^3 + \cdots. \tag{42}$$

We integrate both sides of Eq. (42) in time and find a leading fourth order time dependence of the longitudinal color electric field $E_3^{(3)} = -\partial_t A_3^{(3)}$ according to

$$E_3^{(3)}(t) \simeq \frac{g^2}{4} a_2^{(1)} a_3^{(3)} a_2^{(1)} t^4 + \cdots. \tag{43}$$

Consequently, the longitudinal field energy as defined in Eq. (25) increases as $W_L^{(E)}(t) \sim t^8$ in the leading order of the time dependence. The high power explains why the longitudinal polarization of the receding wave packets is small at short times after the collision but increases rapidly at large times. This time-dependent behavior of $W_L^{(E)}(t)$ together with the resulting transverse expansion of the energy density distribution characterizes the ''glue burst.''

Our numerical results above show that the time-delay of the burst scales essentially as $1/g^2$. This scaling has the following analytic explanation. Each factor $a_c^{(\mu)}$ in Eq. (43) is proportional to g^2 and thus can be separated as

$$a_c^{(\mu)} = \tilde{a}_c^{(\mu)} g^2, \tag{44}$$

where $\tilde{a}_c^{(\mu)}$ is independent on g. This g^2 dependence results from the contribution of the g^2 term in Eq. (37) during the overlap time as discussed above. The equation (43) rereads now

$$E_3^{(3)}(t) \simeq \frac{1}{4} \tilde{a}_2^{(1)} \tilde{a}_3^{(3)} \tilde{a}_2^{(1)} (g^2 t)^4 + \cdots \tag{45}$$

which explains the numerical observation, i.e., $W_L^{(E)}(t) \sim (g^2 t)^8$. As Fig. 4 shows, the burst leads to a peaklike shape in $W_L^{(E)}(t)$ at the burst time. The steep rise of the longitudinal energy is immediately followed by a strong decrease. This behavior has to be explained by the next order in the expansions (40) and (41). The oscillating nature of the solutions suggests that the coefficients b_μ^c have opposite sign as compared to the coefficients a_μ^c. This results in a next to leading order term on the RHS of Eq. (45) which enters into the expansion as

$$E_3^{(3)}(t) \simeq \cdots + \frac{1}{5g^2} (\tilde{b}_2^{(1)} \tilde{a}_3^{(3)} \tilde{a}_2^{(1)} + \cdots)(g^2 t)^5 + \cdots. \tag{46}$$

Due to the higher power in t, this term takes over shortly after the first term has increased the amplitude of $E_3^{(3)}(t)$. The opposite sign, however, turns the total amplitude back. The following drop of the amplitude is stopped by an opposite effect from the next higher order in Eq. (46) and so on.

In Fig. 4, we observe that $W_L^{(E)}(t)$ stays finite and seems to oscillate irregularly around a finite average value after the burst which we denote preliminary as $\overline{W}_L^{(E)}(\infty)$. This average value is independent on g which is explained by Eq. (45). Equation (45) shows that in lowest order in time, g^2 can be completely scaled out with t. As discussed above, the lowest order determines the rise of the first hump in $W_L^{(E)}(t)$ at the beginning of the burst. The rise of the first hump determines the value of $\overline{W}_L^{(E)}(\infty)$.

The above discussion is so far restricted to colliding plane wave packets of Gaussian shape in longitudinal direction. The arguments made in the discussion, however, hold for wave packets of large finite transverse extension where we can neglect surface effects. For small transverse extensions, the discussion is in principle similar but more involved since contributions from the surface can no longer be neglected.

Finally, the case where $\mathcal{A}^{(3)}$ is not small is considered. In the Appendix A, we argue that the source terms on the RHS of Eq. (37) are suppressed by a factor $1/\overline{k_3}$ in the regime of large $\overline{k_3}$. The g^2 term is even suppressed stronger. When $\overline{k_3}$ is not large the order g term on the RHS of Eq. (37) is large and thus $\mathcal{A}^{(3)}$ grows rapidly after the begin of the overlapping. The source terms of order g in the color directions T_1 and T_2 become also large leading to large contributions in these colors in $\mathcal{A}^{(3)}$. The polarization of $\mathcal{A}^{(3)}$ in the third color during the overlap time vanishes therefore when we go to smaller $\overline{k_3}$. The large amplitudes of $\mathcal{A}^{(3)}$ enter into the g^2 terms on the RHS of Eq. (37) leading to rapid growth of these terms during the overlap time. The burst occurs thus already in the overlap region without time delay.

Generally, we may conclude that the time delay increases when we go from small $\overline{k_3}$ to large $\overline{k_3}$. In this context we refer also to Appendix B.

VI. SUMMARY AND OUTLOOK

We have studied time-dependent solutions of the classical Yang-Mills equations which describe the collision of initially polarized wave packets in color space and position space. We have simulated the collisions on a three dimensional gauge lattice numerically applying the Hamiltonian approach of Kogut and Susskind to describe the dynamics of the color fields in SU(2) gauge symmetry. As a function of time, we have calculated the transverse and longitudinal energy densities $w_T^{(E)}(t,x_3)$ and $w_L^{(E)}(t,x_3)$ of the color electric fields. For initially transverse polarized colliding plane wave packets and for colliding finite wave packets as well, the longitudinal energy densities show a strongly time dependent increase in the overlap region around the center of collision but vanish when the wave packets recede. A similar time-dependent behavior was found for the transverse total energy current. A certain time τ after the collision both the longitudinal color electric field energy and the transverse energy current increase rapidly while the distribution $w_T^{(E)}(t,x_3)$ starts simultaneously to decay. Visualizations in three dimensions show that the wave packets suddenly decay fast in a decoherent manner when the time τ is reached. Both, the maximum transverse energy current at total overlap and τ scale like $1/g^2$ but for different reasons. This and also the burst can be explained by analyzing the Yang-Mills equations.

The question arises, whether this pure classical phenomenon could play a role in high energy nucleus-nucleus collisions. In the present calculations each wave packet was carrying an energy of about 10 GeV. The size of the finite wave packets was 10 fm in longitudinal and 8 fm in the transverse directions. The energy of about 10 GeV is close to the upper limit that can be described on a lattice with the constant $a_l = 0.1$ fm for the above size of the wave packet. It is well known experimentally that about half of the energy in a nucleus is carried by glue fields. A ^{208}Pb nucleus at 100 GeV/nucleon carries thus about 10 TeV in glue fields. It would be interesting, to study the pure glue field dynamics classically in colliding finite wave packets each carrying an energy of 10 TeV. This, however, requires extremely small lattice constants and very large numbers of lattice points. The size of the wave packets can be adjusted to the size of colliding Pb nuclei, i.e., it should have an extension of about 11 fm in the transverse directions. Such a description of course is still very rough and would require much improvement in the future. It would also be interesting to perform a Fourier analysis of the collisions in three dimensions for each color separately. There is also hope that Dirac-Fermion fields can be included in the future.

ACKNOWLEDGMENTS

The authors thank S. G. Matinyan for discussions. This work was supported by the U.S. Department of Energy under Grant No. DE-FG02-96ER40495.

APPENDIX A: ANALYSIS OF THE SOURCE TERMS

We discuss the source terms on the RHS of the the Yang-Mills equations which read

$$\partial_\mu \partial^\mu \mathcal{A}^\nu = \partial_\mu \partial^\nu \mathcal{A}^\mu + ig\partial_\mu [\mathcal{A}^\mu, \mathcal{A}^\nu]_- + ig[\mathcal{A}_\mu, \partial^\mu \mathcal{A}^\nu]_- - ig[\mathcal{A}_\mu, \partial^\nu \mathcal{A}^\mu]_- + g^2[\mathcal{A}_\mu, [\mathcal{A}^\mu, \mathcal{A}^\nu]_-]_- . \tag{A1}$$

Since the time-delayed burstlike behavior of the solution occurs also in the case of colliding plane waves, it is sufficient to discuss Eq. (A1) for this case. We argue that wave packets with large but finite transverse extension can be considered as plane waves.

The numerical results presented in the Sec. III have shown that longitudinal energy densities correspond essentially to transverse energy currents. The longitudinal energy densities therefore exhibit the basic feature of the glue burst solution. The corresponding color electric field components are determined by the negative time derivative of the longitudinal components of the gauge fields. We therefore begin with the discussion of the time evolution of these field components and we set $\nu = 3$ in Eq. (A1). Before the collision, both wave packets are polarized in the x_1 direction in Eu-

clidean space. Accordingly, the longitudinal components are $\mathcal{A}^3=0$ before overlap. In the following we focus on the time region where both wave packets start to overlap.[4]

The first term on the RHS of Eq. (A1) contains a sum of four terms

$$\partial_\mu\partial^\mu\mathcal{A}^3=\partial_0\partial^3\mathcal{A}^0+\partial_1\partial^3\mathcal{A}^1+\partial_2\partial^3\mathcal{A}^2+\partial_3\partial^3\mathcal{A}^3. \tag{A2}$$

The first term on the RHS of Eq. (A2) is zero because we use the temporal gauge in which $\mathcal{A}^0=0$. The second term and the third term are zero because $\partial_1\mathcal{A}^1=0$ and $\partial_2\mathcal{A}^2=0$ for plane waves that propagate into the x_3 direction. For $\nu=3$, explicitly considering the contribution from Eq. (A2) on the RHS and expanding the sum on the LHS, Eq. (A1) now reads

$$\partial_0\partial^0\mathcal{A}^3+\partial_1\partial^1\mathcal{A}^3+\partial_2\partial^2\mathcal{A}^3+\partial_3\partial^3\mathcal{A}^3=\partial_3\partial^3\mathcal{A}^3+\cdots. \tag{A3}$$

This shows that the remaining term of the expression (A2) is canceled by the last term on the LHS of Eq. (A3). For plane waves, the second and third term on the LHS are zero. The contributions from the other source terms in Eq. (A1) are indicated by the dots.

The second term on the RHS of Eq. (A1) is zero initially because of two reasons. First, $\mathcal{A}^3=0$ at the very start of the overlapping. The second reason is explained in the following analysis. The term in $\partial_\mu[\mathcal{A}^\mu,\mathcal{A}^3]_-$ corresponding to $\mu=0$ vanishes due to temporal gauge, the $\mu=3$ term vanishes because of the commutator, and the $\mu=1,2$ terms vanish for plane wave packets. Consequently, we find

$$\partial_\mu[\mathcal{A}^\mu,\mathcal{A}^3]_-=0. \tag{A4}$$

By similar arguments and because of $[\mathcal{A}_3,\partial^3\mathcal{A}^3]_-=0$, we obtain

$$ig[\mathcal{A}_\mu,\partial^\mu\mathcal{A}^3]_-=ig[\mathcal{A}_1,\partial^1\mathcal{A}^3]_-+ig[\mathcal{A}_2,\partial^2\mathcal{A}^3]_- +ig[\mathcal{A}_3,\partial^3\mathcal{A}^3]_-=0 \tag{A5}$$

for the third term on the RHS of Eq. (A1).

The fourth term on the RHS of Eq. (A1) plays an important role in the overlap region. According to our calculation for plane waves, we assume that the colliding wave packets are initially polarized in color space in the directions T_1 and T_2, respectively. When the wave packets start to overlap, a superposition of two colors occurs and we obtain

$$\begin{aligned}-ig[\mathcal{A}_\mu,\partial^3\mathcal{A}^\mu]_-&=-ig[(A_\mu^1T_1+A_\mu^2T_2+\dots),\\ &\quad\partial^3(A_1^\mu T^1+A_2^\mu T^2+\dots)]_-\\ &\simeq -ig(A_\mu^1\partial^3A_2^\mu[T_1,T^2]_-\\ &\quad+A_\mu^2\partial^3A_1^\mu[T_2,T^1]_-)\\ &=g(A_\mu^1\partial^3A_2^\mu-A_\mu^2\partial^3A_1^\mu)T_3.\end{aligned} \tag{A6}$$

As long as the wave packets do not overlap, the color indices 1 and 2 refer here at the same time to the contributions of wave packet 1 and 2. First, the case where $\mathcal{A}^{(3)}$ is small during the overlap time is considered. This assumption, as shown further below, is equivalent to the inequality $|A_\mu^3A_3^\mu|\ll|A_\mu^1A_1^\mu|$ and $|A_\mu^3A_3^\mu|\ll|A_\mu^2A_2^\mu|$. The inequalities allow a neglection of the terms $-ig[A_\mu^3T_3,\partial^3(A_1^\mu T^1+A_2^\mu T^2)]_-$ and $-ig[(A_\mu^1T_1+A_\mu^2T_2),\partial^3A_3^\mu T^3]_-$ on the RHS of Eq. (A6). Consequently, excitations of modes in the color subspace span(T_1,T_2) in $\mathcal{A}^3(t,\vec{x})$ are neglected during the overlap time. These components will be included further below where the case of large $|A_\mu^3A_3^\mu|$ is considered. Excitations occur then only in the third color degree of freedom which is the only remaining component in $\mathcal{A}^3$. The remaining term on the RHS in Eq. (A6) acts as a source term for the third color component of the longitudinal gauge field $\mathcal{A}^3(t,\vec{x})$. Its effect is discussed in Sec. IV.

In the following, the g^2 term is analyzed. It splits into

$$g^2[\mathcal{A}_\mu,[\mathcal{A}^\mu,\mathcal{A}^3]_-]_-=g^2[\mathcal{A}_1,[\mathcal{A}^1,\mathcal{A}^3]_-]_- +g^2[\mathcal{A}_2,[\mathcal{A}^2,\mathcal{A}^3]_-]_-. \tag{A7}$$

First, we consider the contribution of the first term on the RHS of Eq. (A7). The second term does not contribute if both wave packets are polarized into the x_1 direction. Otherwise, it would contribute in an analogous manner. Subsequently, according to the convention in Sec. IV, number values of indices in Minkowski-space are denoted in parentheses in order to distinguish from color indices. As argued in Sec. IV, for large enough $\overline{k_3}$ and small enough Δk_3, the longitudinal fields $\mathcal{A}^{(3)}$ are essentially polarized in the T_3-direction in color space after the step one. The contributions to the first and second color direction are therefore neglected. This is sufficient since the $A(3)_3$-component (which is zero initially) becomes always finite in the overlap region as shown above where a finite amplitude remains after the overlapping. Neglecting $A_1^{(3)}$ and $A_2^{(3)}$, we obtain

$$\begin{aligned}[\mathcal{A}^{(1)},\mathcal{A}^{(3)}]_-&\simeq[A_1^{(1)}T^1+A_2^{(1)}T^2+A_3^{(1)}T^3,A_3^{(3)}T^3]_-\\ &=-iA_1^{(1)}A_3^{(3)}T^2+iA_2^{(1)}A_3^{(3)}T^1\end{aligned} \tag{A8}$$

for the inner commutator. Inserting this result into the LHS of Eq. (A7), leads to

[4]Gaussian wave packets start to overlap at infinitely large distances. What we mean by ''starting to overlap'' in this context is the transition from a distance region in which excitations of the amplitude $\mathcal{A}^3$ are exponentially suppressed into a distance region where finite but small excitation (caused by the g^2 term) appear. This transition is located at relatively small distances and has already been outlined in Sec. IV in the discussion of Eqs. (40) and (41).

$$
\begin{aligned}
&g^2[\mathcal{A}_{(1)},[\mathcal{A}^{(1)},\mathcal{A}^{(3)}]_-]_- \\
&\quad = -g^2[\mathcal{A}_{(1)}, iA_1^{(1)}A_3^{(3)}T^2 - iA_2^{(1)}A_3^{(3)}T^1]_- \\
&\quad = g^2A_{(1)}^1A_1^{(1)}A_3^{(3)}T^3 - g^2A_{(1)}^3A_1^{(1)}A_3^{(3)}T^1 \\
&\qquad + g^2A_{(1)}^2A_2^{(1)}A_3^{(3)}T^3 - g^2A_{(1)}^3A_2^{(1)}A_3^{(3)}T^2. \quad \text{(A9)}
\end{aligned}
$$

As soon as the gauge fields obtain a small contribution in the component $A_3^{(3)}$, the spacial component $\mathcal{A}^{(1)}$ starts to change the polarization in color space. In wave packet (1) the components $A_2^{(1)}$ and $A_3^{(1)}$ grow whereas $A_1^{(1)}$ decreases accordingly.[5] In wave packet (2) the components $A_1^{(1)}$ and $A_3^{(1)}$ grow whereas $A_2^{(1)}$ decreases accordingly.

This behavior is explained by the Yang-Mills equation for the first component

$$
\begin{aligned}
\partial_\mu\partial^\mu\mathcal{A}^{(1)} &= \partial_\mu\partial^{(1)}\mathcal{A}^\mu + ig\partial_\mu[\mathcal{A}^\mu,\mathcal{A}^{(1)}]_- \\
&\quad + ig[\mathcal{A}_\mu,\partial^\mu\mathcal{A}^{(1)}]_- - ig[\mathcal{A}_\mu,\partial^{(1)}\mathcal{A}^\mu]_- \\
&\quad + g^2[\mathcal{A}_\mu,[\mathcal{A}^\mu,\mathcal{A}^{(1)}]_-]_-. \quad \text{(A10)}
\end{aligned}
$$

The first term on the RHS of Eq. (A10) does not contribute for plane waves since $\partial^{(1)}\mathcal{A}^\mu = 0$. The second term yields the contributions

$$
\begin{aligned}
&ig\partial_\mu[\mathcal{A}^\mu,\mathcal{A}^{(1)}]_- \\
&\quad = ig[\partial_3A_3^{(3)}T^3 + \cdots, A_1^{(1)}T^1 + A_2^{(1)}T^2 + \cdots]_- \\
&\qquad + ig[A_3^{(3)}T^3 + \cdots, \partial_3A_1^{(1)}T^1 + \partial_3A_2^{(1)}T^2 + \cdots]_- \\
&\quad = -gA_1^{(1)}\partial_{(3)}A_3^{(3)}T^2 + gA_1^{(1)}\partial_{(3)}A_3^{(3)}T^1 \\
&\qquad - gA_3^{(3)}\partial_{(3)}A_1^{(1)}T^2 + gA_3^{(3)}\partial_{(3)}A_2^{(1)}T^1 + \cdots
\end{aligned}
\quad \text{(A11)}
$$

of which the first and third lead to excitations of modes in the color direction T^2 in the wave packet (1). The second and fourth term leads to excitations of modes in the color direction T^1 in the wave packet (2).

We now discuss the g^2 term. Here, $[\mathcal{A}^{(1)},\mathcal{A}^{(1)}]_- = 0$ in the inner commutator and $\mathcal{A}^{(2)} = 0$ for polarized wave packets. For the essential contributions of the inner commutator we find

$$
\begin{aligned}
[\mathcal{A}^{(3)},\mathcal{A}^{(1)}]_- &= [\partial_3A_3^{(3)}T^3 + \ldots, A_1^{(1)}T^1 + A_2^{(1)}T^2 + \cdots]_- \\
&= iA_3^{(3)}A_1^{(1)}T^2 - iA_3^{(3)}A_2^{(1)}T^1 + \cdots \quad \text{(A12)}
\end{aligned}
$$

Inserting the RHS of Eq. (A12) into the g^2 term, we obtain

$$
\begin{aligned}
g^2[\mathcal{A}_\mu,[\mathcal{A}^\mu,\mathcal{A}^{(1)}]_-]_- &= g^2[\mathcal{A}_{(3)},[\mathcal{A}^{(3)},\mathcal{A}^{(1)}]_-]_- \\
&= g^2A_3^{(3)}A_3^{(3)}A_1^{(1)}T^1 \\
&\quad + g^2A_3^{(3)}A_3^{(3)}A_2^{(1)}T^2 + \cdots. \quad \text{(A13)}
\end{aligned}
$$

It has to be shown that in the regime of large $|\overline{k_3}|$, the condition of small $\mathcal{A}^{(3)}$ during the overlap is equivalent to the conditions $|A_\mu^3A_3^\mu| \ll |A_\mu^1A_1^\mu|$ and $|A_\mu^3A_3^\mu| \ll |A_\mu^2A_2^\mu|$. With the above equation (A6) follows

$$
\partial_{(0)}\partial^{(0)}\mathcal{A}^{(3)} \simeq g(A_\mu^1\partial^{(3)}A_2^\mu - A_\mu^2\partial^{(3)}A_1^\mu)T_3 \quad \text{(A14)}
$$

for the overlap region. From the inequalities follows directly that $|A_3^{(3)}|$ is small. This amplitude enters into the g^2 term of Eq. (A10). From Eq. (A13) together with Eq. (A6) follows that the g^2 term is quadratically small in $A_3^{(3)}$. Consequently, the g^2 term is neglected in Eq. (A12). At the begin of the overlap $\mathcal{A}^{(3)}$ is zero. From Eq. (A12) follows that only the third color component in $\mathcal{A}^{(3)}$ grows during the overlap time. For large $|\overline{k_3}|$ and for wave packets defined by the initial conditions (16) to (18) the operator $\partial^{(3)}$ is approximately replaced by a factor $\overline{k_3}$. Further, two time integrations of Eq. (A12) lead to an additional factor $\overline{k_3}^{-2}$. The RHS of Eq. (A12) is therefore suppressed by a factor $1/\overline{k_3}$ in the regime of large $\overline{k_3}$. Consequently, the source term on the RHS of Eq. (A12) is small and thus the field amplitude $\mathcal{A}^{(3)}$ remains small accordingly.

The inverse conclusion is provided by the condition that $\mathcal{A}^{(3)}$ is small. It has to be shown that $A_3^{(1)}$ and $A_3^{(2)}$ are small. $\mathcal{A}^{(3)}$ enters linearly into the RHS of Eq. (A11) and quadratically into the RHS of Eq. (A13). The generators T_c are linearly independent in LSU(2). Therefore Eq. (A10) represents a system of three equations, one for each T_c. The RHS of the equation for the third color is composed by all T_3 terms on the RHS of Eq. (A11) and Eq. (A13). Each of these terms contains at least one factor $A_3^{(3)}$. The source terms on RHS of Eq. (A10) in the third color direction are therefore small and consequently $A_3^{(1)}$ on the LHS remains small. For large $\overline{k_3}$, this trend is even enhanced by the $1/\overline{k_3}$ behavior of $A_3^{(1)}$ with the above initial conditions. $A_3^{(2)}$ is zero since $\mathcal{A}^{(2)}$ is zero throughout the whole collision. This follows obviously from Eq. (A10) when we replace the explicit space index (1) by the space index (2). All terms on the RHS which contain $\mathcal{A}^{(2)}$ remain zero. Further, the derivatives $\partial^{(2)}\mathcal{A}^\mu$ are zero for colliding plane waves.

APPENDIX B: TIME DELAY AT LARGE MOMENTA

In this appendix, we briefly discuss the $\overline{k_3}$-scaling in the overlap region and in the burst region. As discussed in Sec. IV, for not too large g, the fourth term on the RHS in the equation

[5] Since the fields of the original wave packets are superposed (in a non-linear manner) in the overlap region, it is subtle to talk in terms of wave packets. For initially polarized wave packets, one can essentially distinguish between the field contribution of wave packet (1) and wave packet (2) during full overlap when $|A_3^{(3)}|$ is much smaller than $A_1^{(1)}$ and $A_2^{(1)}$. Field modes which are excited during overlap do not belong to any wave packet during overlap. Such modes are distributed around $\overline{k_3} = 0$ in momentum space.

$$\partial_\mu \partial^\mu \mathcal{A}^\nu = \partial_\mu \partial^\nu \mathcal{A}^\mu + ig\partial_\mu [\mathcal{A}^\mu, \mathcal{A}^\nu]_- + ig[\mathcal{A}_\mu, \partial^\mu \mathcal{A}^\nu]_- - ig[\mathcal{A}_\mu, \partial^\nu \mathcal{A}^\mu]_- + g^2 [\mathcal{A}_\mu, [\mathcal{A}^\mu, \mathcal{A}^\nu]_-]_- \tag{B1}$$

acts as the dominant source term for the longitudinal field components in the overlap region of the colliding wave packets. We treat Eq. (B1) first for $\nu = 3$. Assuming that during the overlap time the wave packets deviate not much from their initial form

$$\phi(t, x_3) = \phi_0 \exp\left(-\frac{1}{2} \Delta k_3^2 (t + x_3)^2 \right) \cos[\overline{k_3}(t + x_3)], \tag{B2}$$

we can make the approximation $\partial^{(3)} \mathcal{A}^\mu \simeq \overline{k_3} \mathcal{A}^\mu$ at large $\overline{k_3}$. At large $\overline{k_3}$, the evolution of the field component $\mathcal{A}^{(3)}$ during the overlap is described by Eq. (37). Omitting the g^2 term on the RHS of Eq. (37), the equation reads

$$\partial_0 \partial^0 \mathcal{A}^{(3)} \simeq g(A_\mu^1 \partial^{(3)} A_2^\mu - A_\mu^2 \partial^{(3)} A_1^\mu) T_3. \tag{B3}$$

In the overlap region, the differentiation $\partial^{(3)}$ in the source term is replaced by a factor $\overline{k_3}$. After two time integrations of Eq. (B3) the RHS obtains an additional factor $1/\overline{k_3^2}$. This shows that the amplitude $\mathcal{A}^{(3)}$ is proportional to $1/\overline{k_3}$ during the overlap time. The height of the hump in $w_L^{(E)}(t,z)$ follows therefore a $1/\overline{k_3^2}$ scaling in the overlap region. Further, $\mathcal{A}^{(3)} \sim \overline{1}/k_3$ enters into the g^2 term on the RHS of Eq. (B1). Consequently, the coefficients $\tilde{a}_c^\mu$ which appear in Eq. (45) in the section 4, depend as $\tilde{a}_c^\mu \sim 1/\overline{k_3}$ on $\overline{k_3}$. Separating factors $1/\overline{k_3}$ from the coefficients leads to

$$E_3^{(3)}(t) \simeq \frac{1}{4} \overline{a}_2^{(1)} \overline{a}_3^{(3)} \overline{a}_2^{(1)} (g^2 \overline{k_3}^{-3/4} t)^4 + \cdots \tag{B4}$$

with new coefficients $\overline{a}_c^\mu = \tilde{a}_c^\mu \overline{k_3}$. We conclude that the time delay of the burst scales as $\overline{k_3}^{3/4}$.

[1] J. P. Blaizot and A. H. Mueller, Nucl. Phys. **B289**, 847 (1987).

[2] M. Gyulassy and X.-N. Wang, Phys. Rev. D **44**, 3501 (1991); X.-N. Wang, Phys. Rep. **280**, 237 (1996).

[3] K. Geiger and B. Müller, Nucl. Phys. **B369**, 600 (1992); K. Geiger, Phys. Rep. **258**, 237 (1995).

[4] T. S. Biró, E. van Doorn, B. Müller, M. H. Thoma, and X.-N. Wang, Phys. Rev. C **48**, 1275 (1993).

[5] L. Xiong and E. V. Shuryak, Phys. Rev. C **49**, 2203 (1994).

[6] A. Makhlin and E. Surdutovich, Phys. Rev. C **58**, 389 (1998).

[7] L. McLerran and R. Venugopalan, Phys. Rev. D **49**, 2233 (1994); **49**, 3352 (1994).

[8] A. Kovner, L. McLerran, and H. Weigert, Phys. Rev. D **52**, 3809 (1995); **52**, 6231 (1995).

[9] J. Jalilian-Marian, A. Kovner, L. McLerran, and H. Weigert, Phys. Rev. D **55**, 5414 (1997); J. Jalilian-Marian, A. Kovner, A. Leonidov, and H. Weigert, Nucl. Phys. **B504**, 415 (1997); J. Jalilian-Marian, A. Kovner, and H. Weigert, Phys. Rev. D **59**, 014015 (1999).

[10] A. Krasnitz and R. Venugopalan, Report No. NBI-HE-97-26, hep-ph/9706329; Report No. NBI-98-22, hep-ph/9808332; Report No. NBI-98-21, hep-ph/9809433.

[11] S. A. Bass, B. Müller, and W. Pöschl, Report No. DUKE-TH-98-168, nucl-th/9808011.

[12] W. Pöschl, B. Müller, Report No. DUKE-TH-98-169, nucl-th/9808031.

[13] C. R. Hu *et al.*, Phys. Rev. D **52**, 2402 (1995).

[14] C. Gong, S. G. Matinyan, B. Müller, and A. Trayanov, Phys. Rev. D **49**, 607 (1994).

[15] L. D. Landau and I. J. Pomeranchuk, Dokl. Akad. Nauk SSSR **92**, 535 (1953); **92**, 735 (1953); english translation in *The Collected Papers of L. D. Landau* (Pergamon, New York, 1965), Secs. 75–76, pp. 586–593; A. B. Migdal, Phys. Rev. **103**, 1811 (1956).

[16] W. Pöschl and B. Müller, Report No. DUKE-TH-99-184, nucl-th/9903050.